Aspects of the Seismic Response to Shaft Pillar Mining - Case Studies in the Welkom Gold Field

DR G VAN ASWEGEN
Welkom Gold Mine

INTRODUCTION

Several shaft pillars have lately been mined out in the Welkom gold field and a number still have to be mined. In this contribution, some of the experience gained by the seismic monitoring of the rockmass response is described. Three cases, all from Western Holdings Mine, are considered, namely shafts no. 6, 2 and 4. The mining is complete in the first two cases and is more than half way in the case of the last.

The seismic response is described in terms of seismic time histories and statistical hazard parameters. In the time history analyses, cumulative apparent volume (åVa) and median energy index (EI) are used to compare the stress and strain histories of the pillars and to establish benchmark cases for future reference to shaft pillar mining under these conditions. These and other seismic parameters are defined in Appendix 1.

MINING ENVIRONMENT

The Basal Reef is the ore body in each case and the depth, reef dip and structural complexities are broadly similar. Figure 1 is a plan of a part of the mine, showing the shaft positions relative to regional mining faces, while more detail is given in Figures 8-10. Table 1 summarises some of the characteristic features of the shafts.

The shafts were mined 'conventionally', i.e. from the inside out. The design was largely based on stress modelling. Backfill was

used in part. More details of the shaft pillar mining is given in a compilation by Lategan (1996).

SEISMIC TIME HISTORIES

In this section, the seismic histories of the shafts are described in terms of seismic event parameters cumulative apparent volume (åVa), apparent stress (sA) and energy index (EI). The stress/strain history of No. 6 Shaft, as inferred from seismicity, has been described as similar to that of a rock sample in a laboratory press (see van Aswegen et al, 1997, p.226): an initial period of 'strain hardening', characterized by relatively low seismic strain rate (as indicated by the slope of the åVa curve) and high moving median energy index followed by 'softening', when the seismic strain rate increased significantly and the EI dropped. The shaft area reached a peak stress level around May 1993 before it dropped relatively sharply. The slope of the åVa increased after May '93 and remained high till the end 1994 when mining was completed. Most of the largest seismic events occurred after May 1993.

Table 1
Some characteristics of the pillars of Shafts No. 2, 4 & 6, Western Holdings Mine

SHAFT	AVG. DEPTH [M]	DIP	APPR. AREA [M^2]	STRUCTURAL FEATURES
6#	1 300	15°	0.7E5	Fault bound in the east, minor fault, steeply dipping to the north, cuts through centre.
2#	950	25°	1.3E5	Major fault/dyke/sill bound on a ll sides, NS faulting through centre, structurally most complex.
4#	1 430	16°	1.6E5	Pillar 'cut loose' from major dyke at western boundary, NE fault/dyke/horst zone cuts through centre.

For the purpose of the time history study, seismic data (and production data in the case of No.'s 2 and 4 Shafts) were selected from within the boundaries of the shaft pillars only, i.e. seismic events spatially associated with major structures outside the pillars were excluded (Figures 8 - 10).

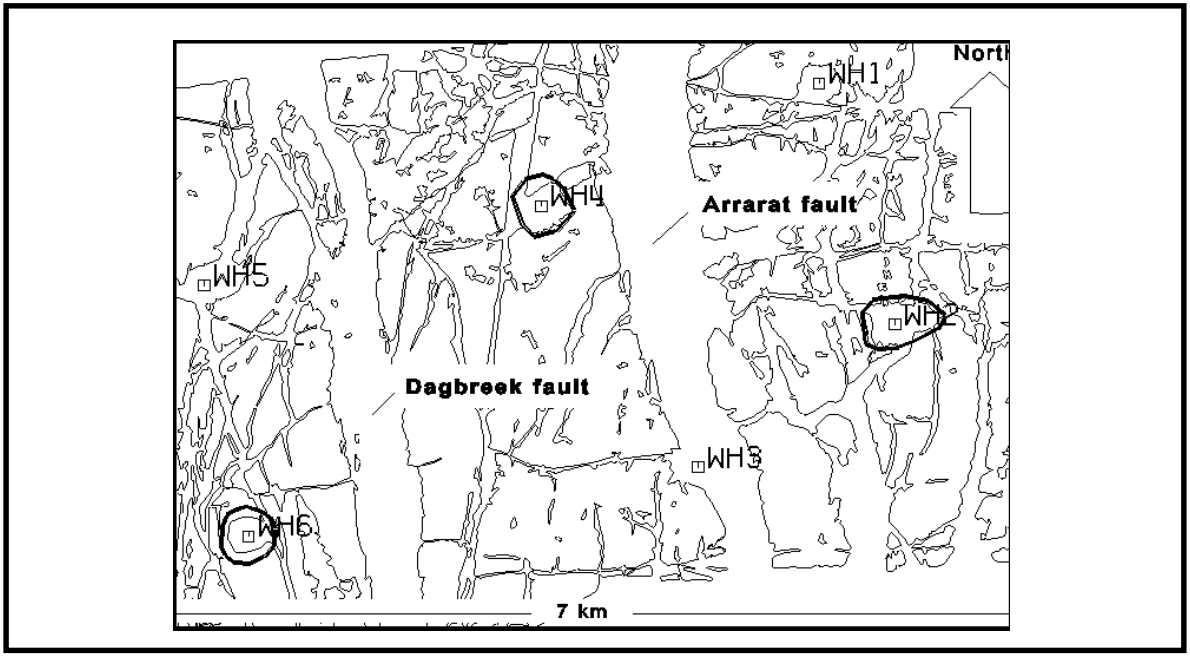

Figure 1

Mining faces of a largely mined out part of Western Holdings Mine depict two major faults loss areas and six shaft pillars. Data for this study were selected from the three polygons shown around Shafts No. 2, 4 and 6

Time histories of åVa and moving median EI for the three shafts considered here are shown in Figures 2, 3 and 4. The time scale for all these plots are the same apart for a two-year time shift between No. 6 Shaft (1/1/90 - 28/5/95) compared to No.'s 2 and 4 (1/1/92 - 28/5/97).

Larger events are shown as vertical lines on the time history diagrams.

Note that the two shafts at which mining is complete (No.'s 6 and 2, Figures. 2 and 3) show very similar time history patterns, i.e. the 'stress-strain' history described for No. 6 Shaft was repeated at No. 2 Shaft. Note also that, in comparison with the two mined out shafts, No. 4 Shaft is already in the high strain rate stage and has apparently passed its peak level of EI.

In Figures 2 to 4 the vertical scales are not fixed. The EI is based on local empirical E-M relations and cannot be compared between shafts.

The seismic strain rate should generally follow production rate. Figures 5 and 6 compare production rate and åVa of No.'s 2 and 4 Shafts. In this case the vertical scales are held constant to show that, at No. 4 Shaft, a larger area has already been mined compared to the total at No. 2 Shaft, explaining the greater åVa value. Note how the åVa slope correlates with that of production at both shafts.

To further compare the seismicity at No. 2 and 4 shafts, the 'stress level' as indicated by the Apparent Stress Level for moment = 1E10 N.m. ($s_A < M^{10} >$ see Appendix 1 where this term is introduced) was calculated for different time periods:

- Up to the end of 1993, both shafts, (for the background level prior to significant shaft pillar mining);

- 01/12/95 - 31/05/95 for 2#, 1/07/96 - end for 4# to coincide with the periods of peak production (compare Figures 5 and 6);

- 01/01/97 - end, both shafts, to compare the final stage of 2#

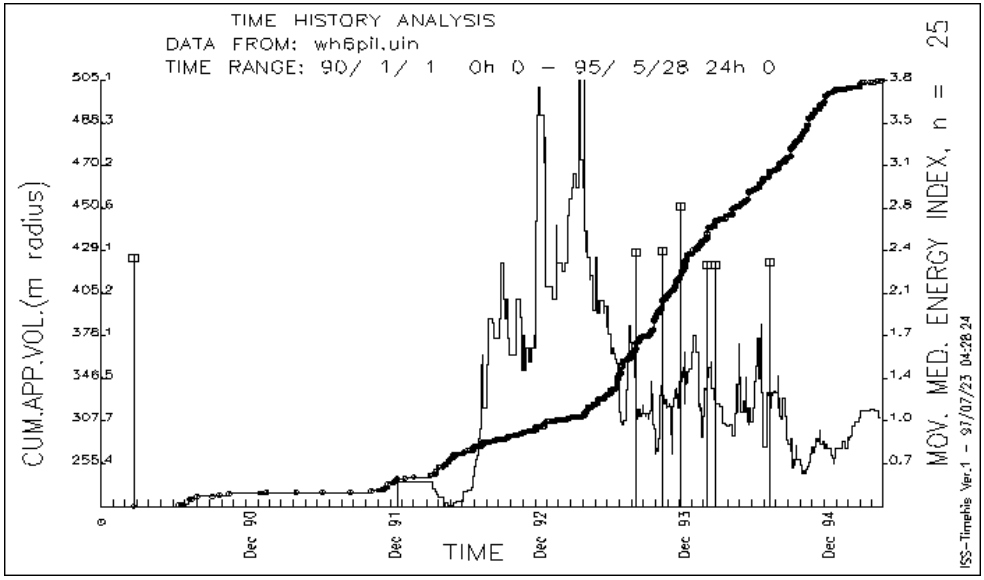

Figure 2

Time history of åVa and moving median EI for the period 01/01/90 to 28/05/95, WH#6

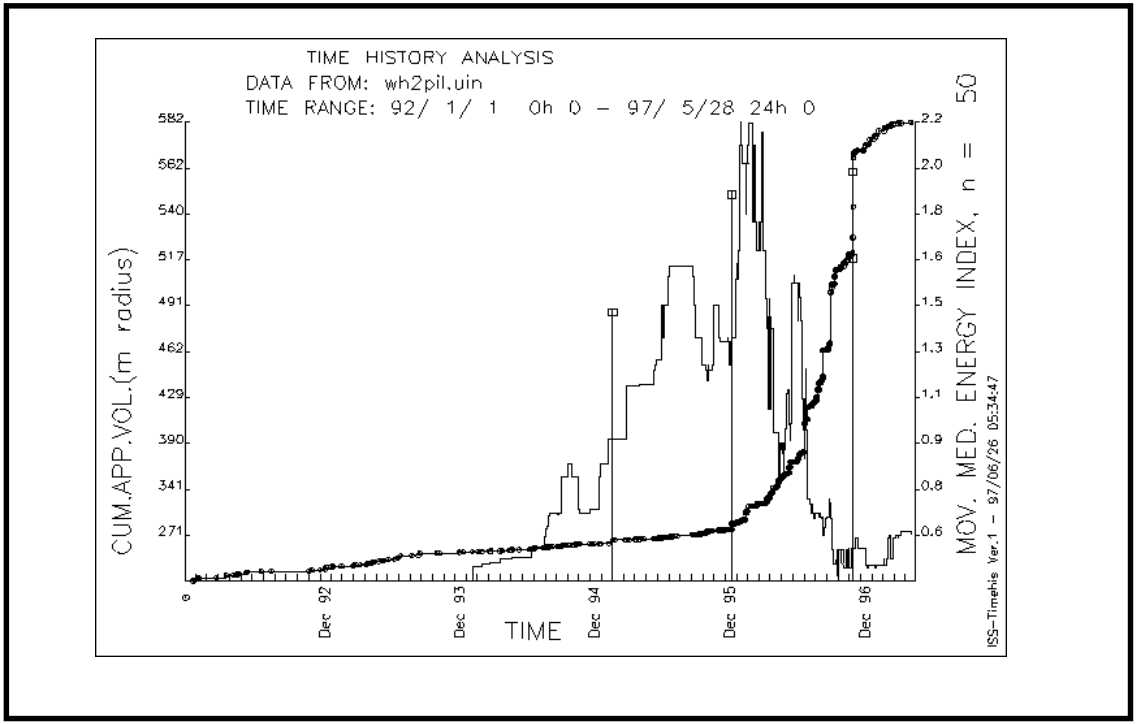

Figure 3

Time history of åVa and moving median EI for the period 01/01/92 to 28/05/97, WH2#

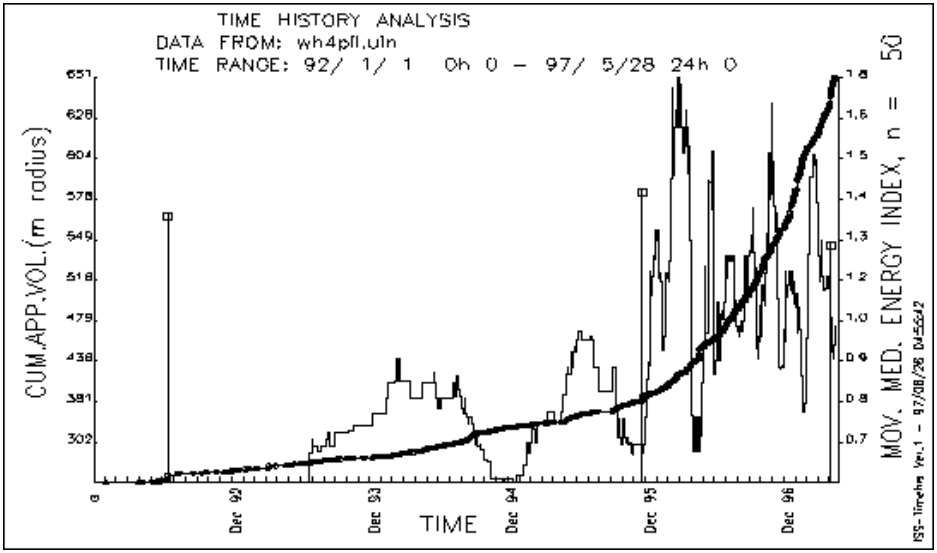

Figure 4

Time history of åVa and moving median EI for the period 01/01/92 to 28/05/97, WH4#

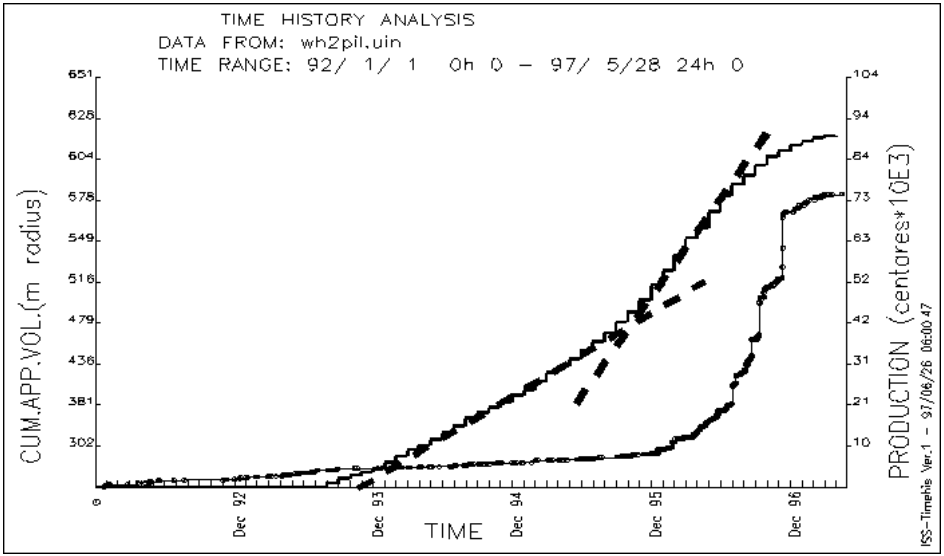

Figure 5

Time history of cumulative production and cum.V for the No. 2 shaft pillar. The broken lines accentuate production rates for particular periods

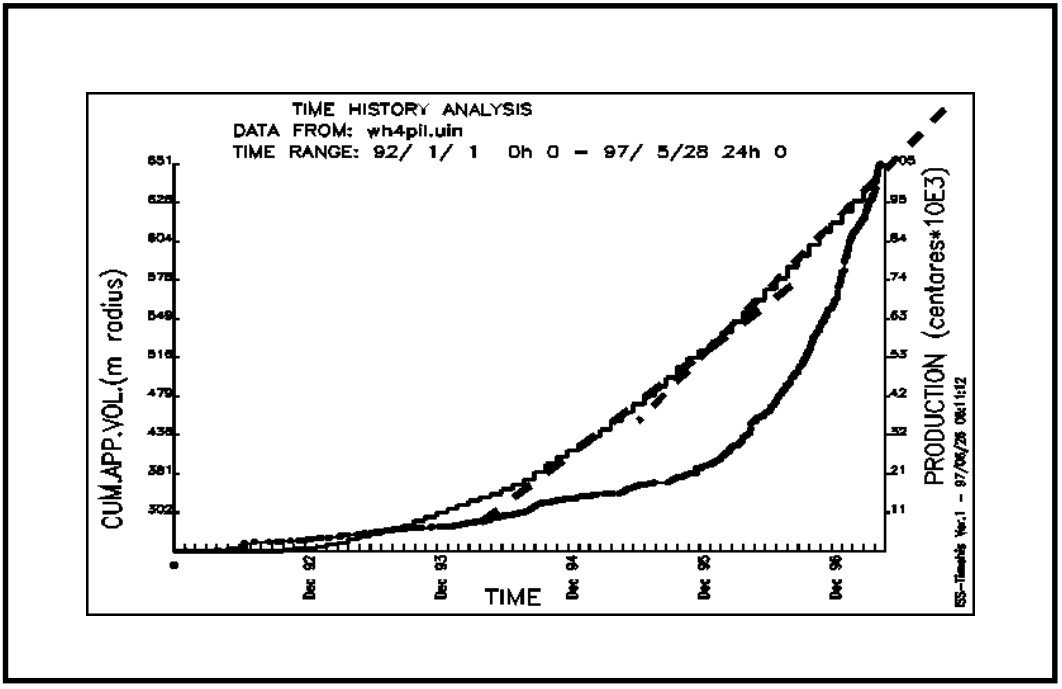

Figure 6

Time history of cum.Va and cumulative monthly production for WH4# during the period 01/01/92 - 28/05/97

with the late phase of 4#.

The E-M empirical fit for the first period at No. 4 Shaft is shown in Figure 7. The results of the calculations are given in Table 2. Note that, prior to the main pillar mining stages, this seismic stress indicator shows a higher value for 4# than for 2#. However, during the high production rate stage, the Apparent Stress Level at 2# is double that at 4#. During the dying stage of 2# the value has dropped some, but it still remained higher than at 4#. It was also noted that the seismic event size and apparent stress distribution at No. 2 Shaft was distinctly skew. The main population of seismic events define the empirical E-M relations on which the first row of Table 2 is based.

A second population is characterised by low E/M values and a $\overline{\sigma_A}\langle M^{10}\rangle$ value of 20 KPa. (see Figure 7).

Table 2

Apparent Stress Level, i.e. average apparent stress for Log (M)=10 ($\overline{\sigma_A}\langle M^{10}\rangle$) for different stages of mining at WH No.'s 2 and 4 Shafts. The units are KPa.

SHAFT	PRE PILLAR MINING	DURING PEAK PRODUCTION	FINAL STAGE (2#)/ LATE STAGE (4#)
2#	21	40	35
4#	29	20	20

NOTE: Comparisons of $\overline{\sigma_A}\langle M^{10}\rangle$ is less reliable along the rows than the columns since the seismic monitoring system has improved significantly through time - the way source parameters (like E and M) are calculated changed as a result.

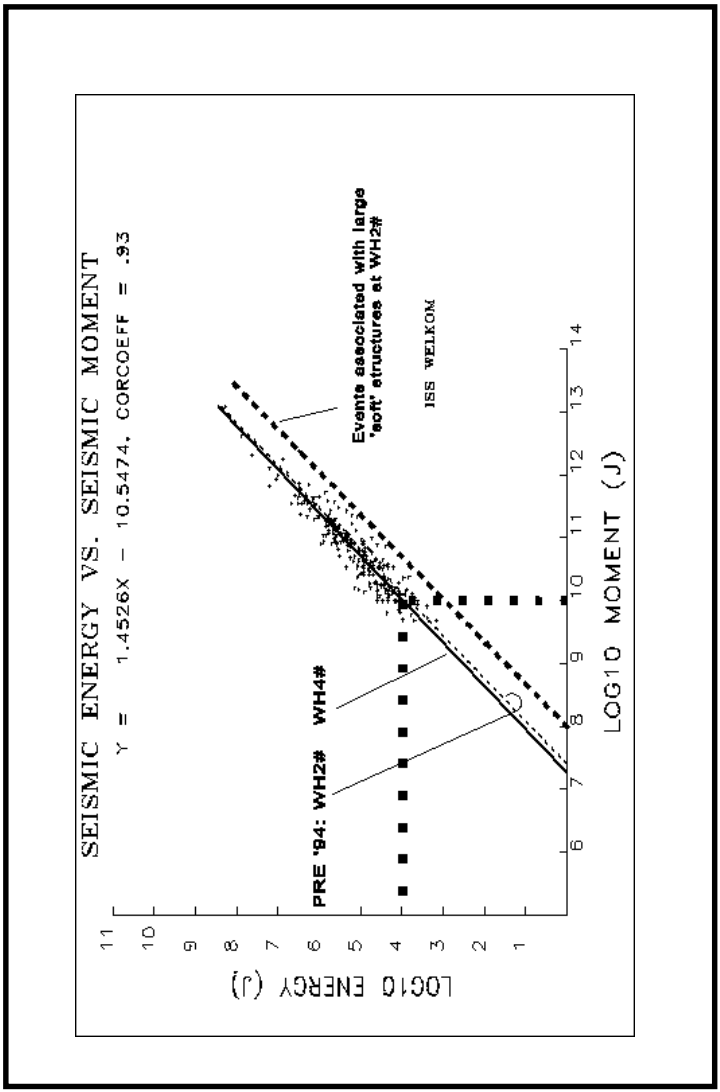
SEISMIC ENERGY VS. SEISMIC MOMENT
Y = 1.4526X - 10.5474, CORCOEFF = .93
LOG10 ENERGY (J)
LOG10 MOMENT (J)
PRE '94: WH2# WH4#
Events associated with large 'soft' structures at WH2#
ISS WELKOM

Figure 7

SEISMIC HAZARD

Seismic hazard is defined as the probability that a seismic event of given magnitude or greater will occur within a given time (seismic risk being the product of hazard and liability). The classical way of describing the magnitude distribution of seismic events and hence estimating seismic hazard is through the so-called Gutenberg-Richter analysis. The principle is simply that the sizes (magnitudes) of seismic events follow a fractal distribution. The number of events decrease exponentially with size. Describing this phenomenon for a given area is done through a cumulative frequency versus magnitude plot, such as shown in Figures 7 onwards.

The Gutenberg-Richter relation has the form log ån = a - bm, where n is the number of events with magnitude m and greater. The negative sign is used in the relation so that the coefficient b is quoted as a positive value, i.e. the b-value. If the event frequency increases, the value of an increase, if the proportion of larger relative to the smaller events increases, the b-value decreases. A b-value of 1.0 is considered 'normal'. Other parameters of concern are Mmax (maximum magnitude) and Mmin (minimum magnitude for which the data base is complete). Having established these coefficients for a given area/ time, the seismic hazard can be calculated and presented in the form of probability and recurrence timetables. The methods used here are as proposed in Mendecki et al, 1995.

Evidently, part of the rockmass response to pillar mining is the de-stabilization of large geological structures immediately adjacent to the pillars. To capture this effect in the statistical analysis of the data, slightly larger polygons were chosen for event selection compared to those for the time history analyses. Figures 8, 9 and 10 are simplified plans of the shaft pillar areas, showing the most important geological features, the event selection polygons and some of the larger events, which were recorded. For WH2# and WH4#, two time periods were chosen for inclusion here.

The first period in each case represents the seismic pre-history in the immediate surrounds of the pillar as well as some of the preparatory mining of the pillars, in each case leading to the first local magnitude

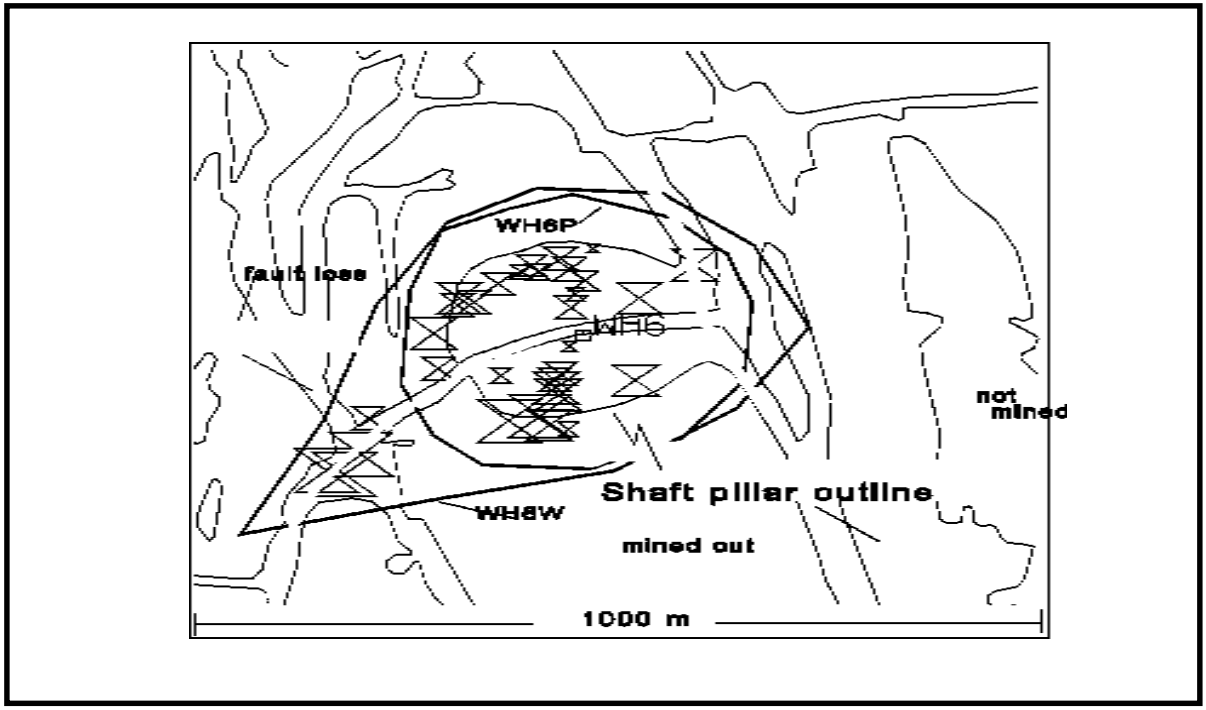

Figure 8

Important geological features, event selection polygons and some of the larger events recorded at WH6#. The mining faces are as they were prior to mining in the pillar.

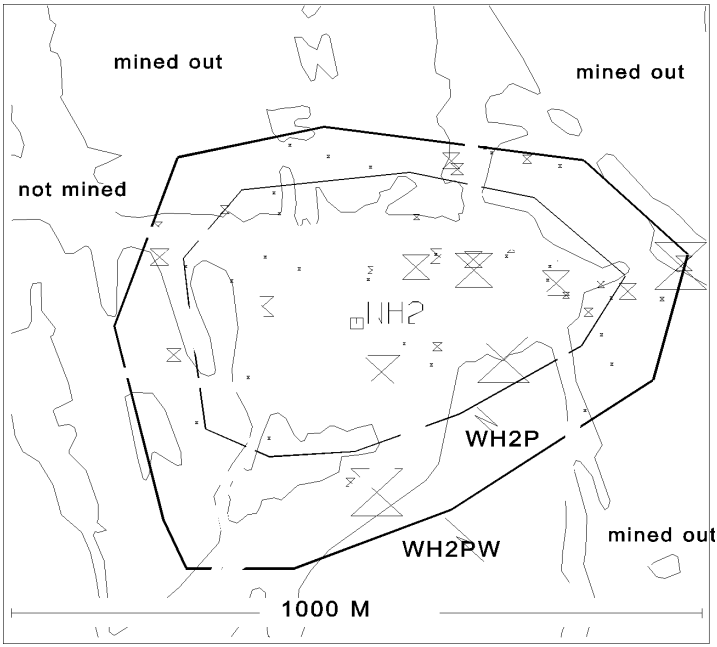

Figure 9

Important geological features (schematic), event selection polygons and some of the larger events recorded at WH2#. The mining faces are as they were prior to mining in the pillar.

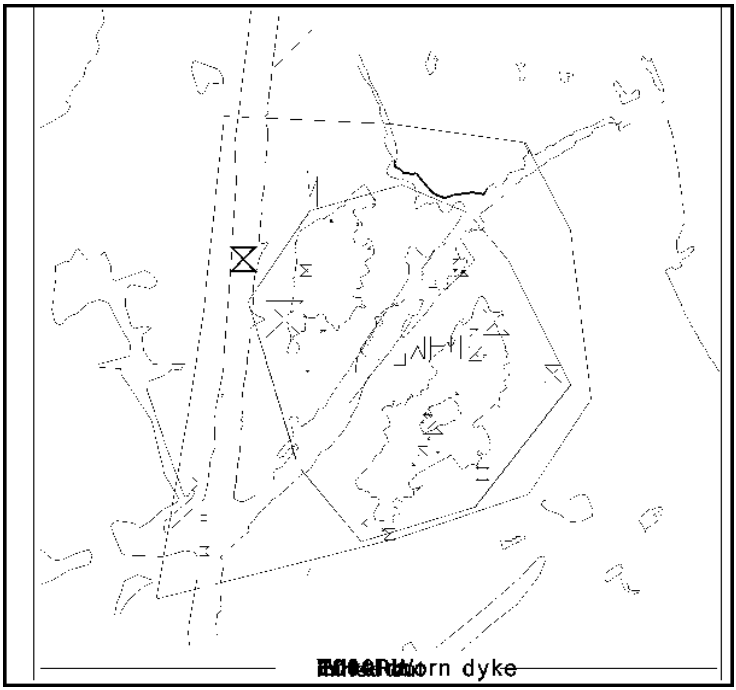

Figure 10

Important geological features, event selection polygons and some of the larger events recorded at WH4#. The mining faces are as they were at the approx. 60% extraction stage.

2 event. The purpose was to see whether there was information in these statistics pertaining to the subsequent seismic response to pillar mining. In the case of WH2# the end date for this period was chosen to be end February 1995 while for WH4# the end of Dec 1995 was used - i.e. the times at which the maximum change in strain rate, as depicted by the slope of åVa curve occurred. The second time period in each case was 01/11/96 - end June 1997 to capture the tail end of the WH2# production and to ensure compatibility of data in the light of recent changes in source parameter calculation methods. The results of the statistical analyses of the different data sets are given in Figures 11 - 15 and in Table 3.

Table 3

b-Value, recurrence times (Rt, in months) and probability of occurrence (within 1 month) for mag.m or larger events for stages: before main pillar mining stage (-B), late/final stage (-F) and total period (-T). F1 and F2 refer to the two populations of events at WH2#.

	b	Rt m2	P.m2	Rt m3	P.m3
WH6-T	0.94	1.90	.41	21.0	.05
WH2-B	0.88	5.12	.18	58.4	.02
WH2-F2	0.44	2.89	.32	12.04	.09
WH2-F1	1.86	>99	.01	>99	0.0
WH4-B	1.03	3.14	.27	>99	0.001
WH4-F	0.99	1.78	.43	>99	0.0

From these, some observations can be made. The size distributions of events at WH6# and WH4# are close to 'normal', with a b-value close to 1.0. In the case of WH4, this remained the case after mining a large part of the shaft pillar (> 50%). In the case of WH2#, the b-value was initially low, but the response to the pillar extraction was the yielding of two populations of events, the larger events displaying a very low b-value, causing a concave downward bend of the cum. frequency-magnitude plot. A comparison of Figure 12 with Figure 13 shows that a tendency for the cum. frequency-magnitude plot to flatten with increase in magnitude, became accentuated during and after shaft pillar extraction.

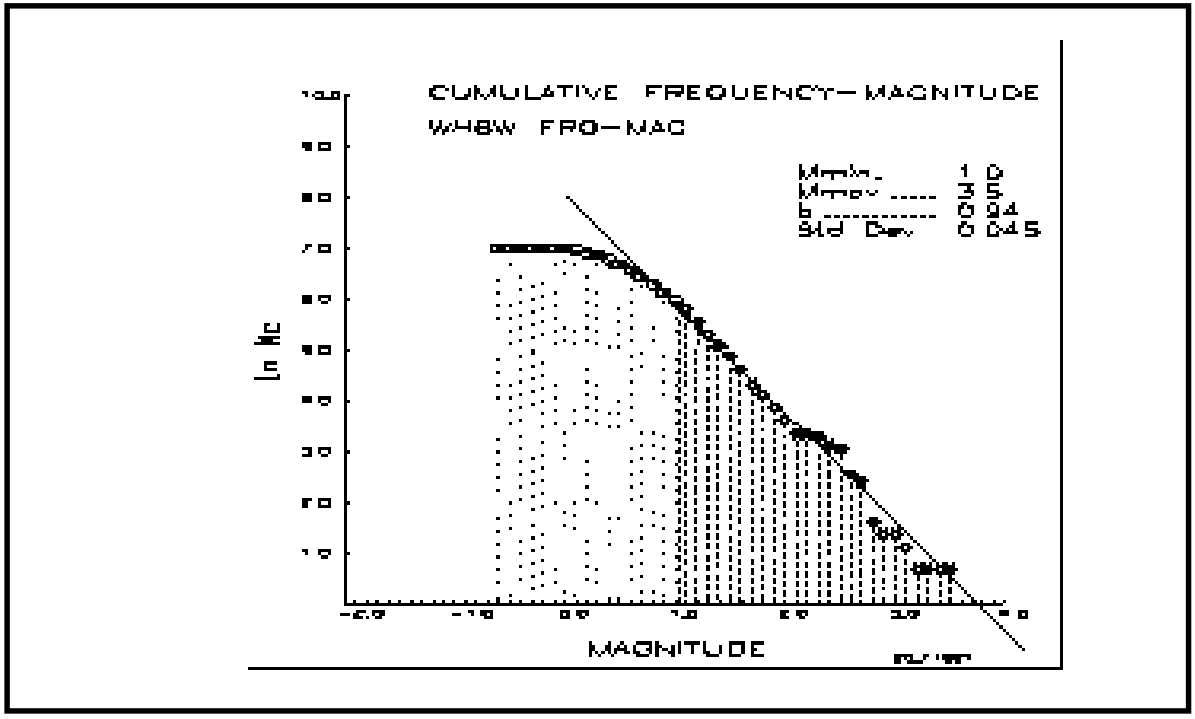

Figure 11

Frequency-magnitude plot for seismic data from WH6 for the period Jan '90 - Mar '95

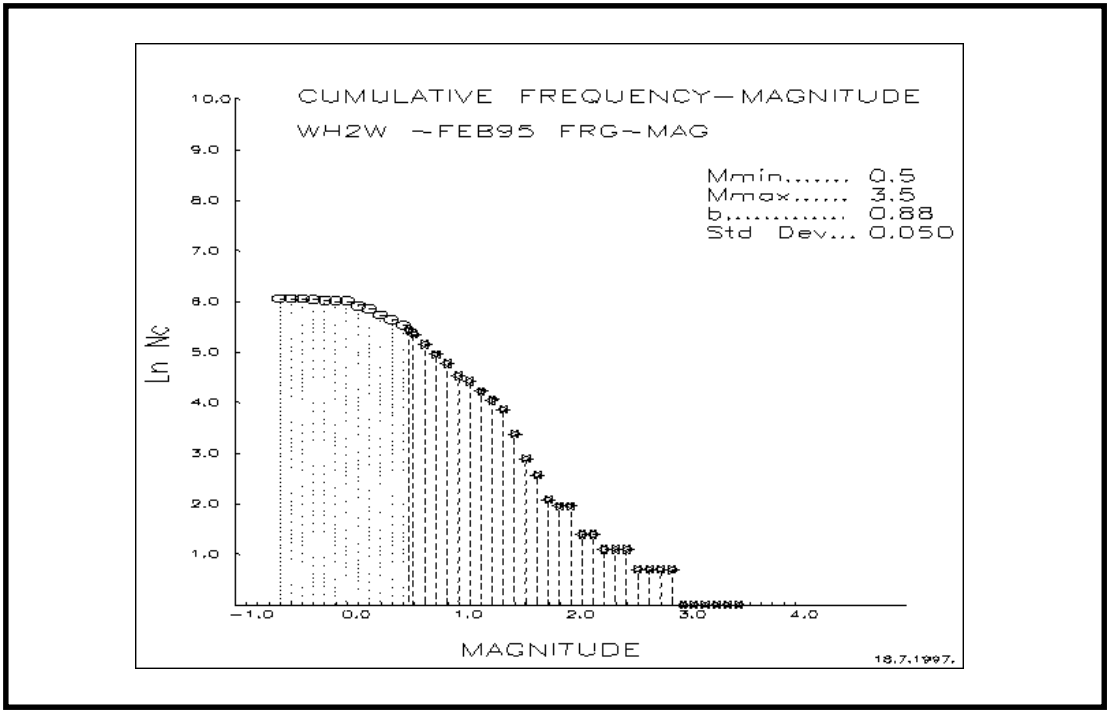

Figure 12

Cumulative frequency-magnitude plot for WH2# for the period 01/01/90 till 28/02/95.

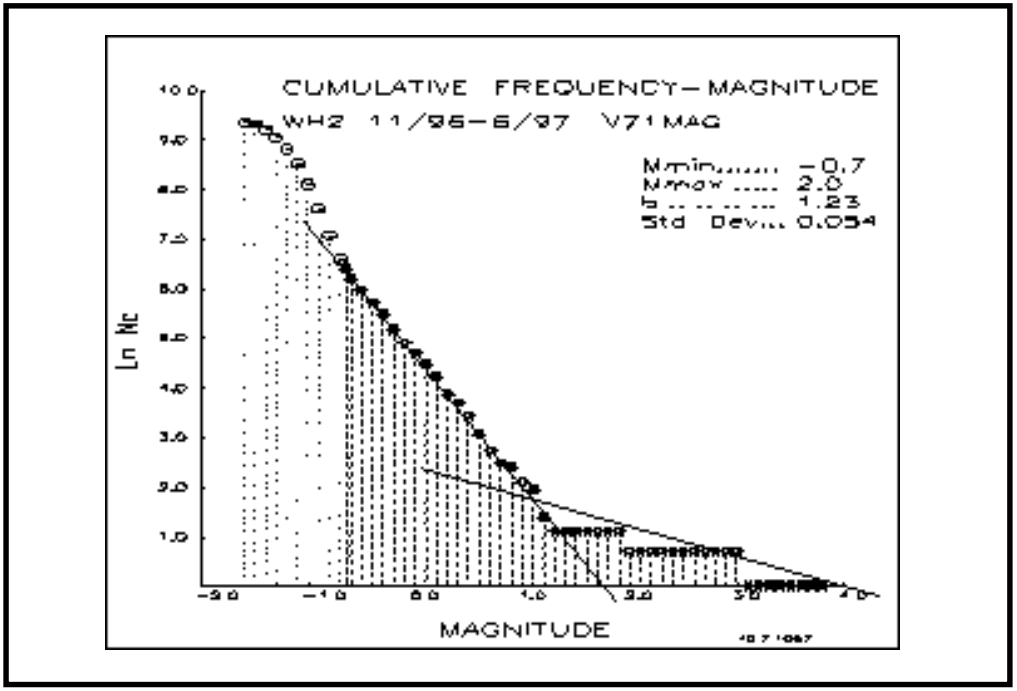

Figure 13

Cumulative frequency-magnitude plot for WH2# for the period 01/11/96 till 30/06/97.

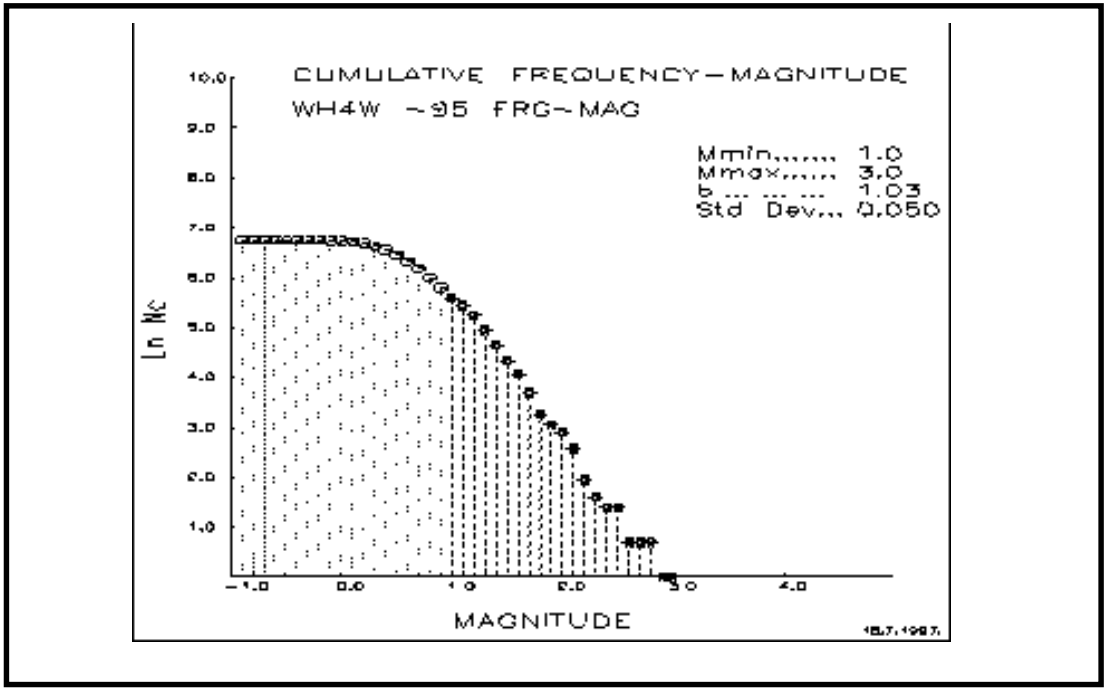

Figure 14

Cumulative frequency-magnitude plot for WH4# for the period 01/01/90 till 31/12/95.

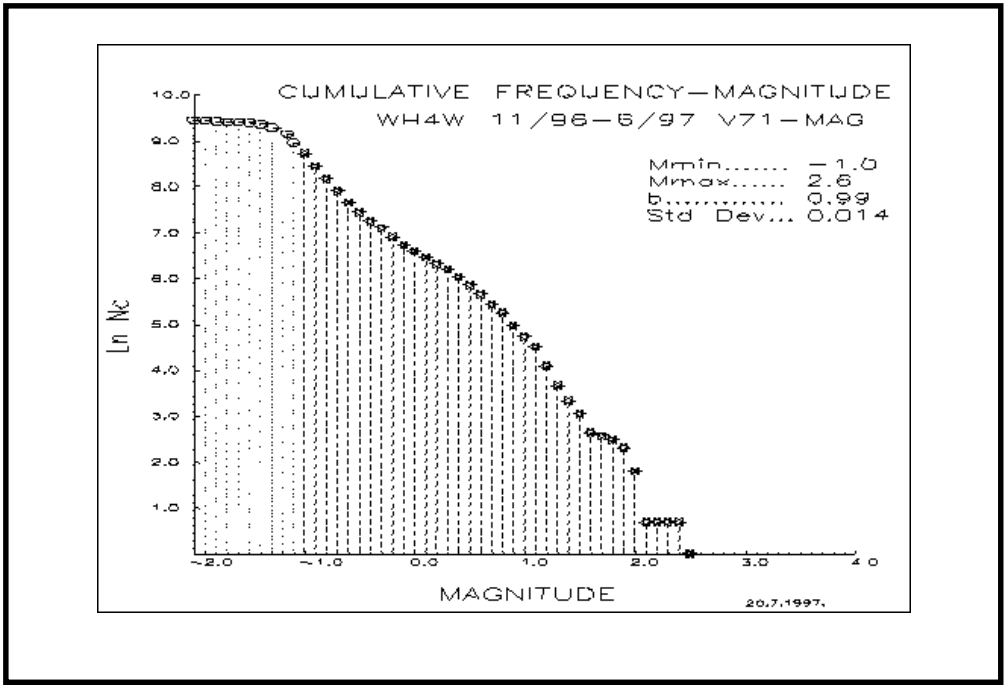

Figure 15

Cumulative frequency-magnitude plot for WH4# for the period 01/11/96 till 30/06/97.

DISCUSSION AND CONCLUSIONS

The similarities in the stress-strain patterns as indicated by $\sum V_A$ and median EI, namely an initial stage of increase in stress level and then a drop associated with increased strain rate, shows that this phenomenon, first described for WH6#, is generally to be expected during shaft pillar extraction. It is not surprising - the seismic source parameters merely reflect the expected variations in stress and strain rate associated with a rapidly decreasing pillar size. It does, however, provide a tool to monitor the timing of these variations.

The differences in stress level between WH2# and WH4# at different stages, as indicated by $\sigma_A < M^{10} >$, requires some consideration. Since WH2# is shallower, the initial lower value here is expected. The subsequent higher stress level is unexpected. It may result from a higher production rate at 2# - compare the slopes of the cumulative production curves in Figures 5 & 6.

The skew size distribution of seismic events at 2# could be explained by the response of geological structures to production. Larger events are generally associated with major faults or dykes while the smaller events are the direct response of the rockmass in general to the stress induced by stoping. Bi-modal event size distribution is not unknown in mines (e.g. Kjiko, 1987) and the explanations are generally the same. The relatively low E/M ratios of the larger events at WH2# (Figure 7) indicates a 'soft' nature for the larger structures. It suggests that it is the large faults, with known weak fault rock filling, that slip to yield the larger events rather than some of the stiffer dykes. Rockburst damage was associated with dykes (as observed after the largest event in Dec. 1996), but the low σ_A of the events, which caused the damage suggested relatively 'slow' tremors. The dyke bursting is explained as a local response to the dynamic loading caused by the large tremor.

At WH4#, the most prominent geological structure is the strong (compared to the surrounding quartzites) 30m wide Enkeldoorn dyke. In contrast, the most prominent geological structure at WH2# is a weak, large displacement fault. This probably exemplifies the general difference in geological structure between the two shafts as reflected

at an early stage by the lower b-slope for the larger events prior to main pillar extraction at WH2# - compare Figures 12 and 14. The potential seismic hazard posed by the Enkeldoorn dyke, a structure known as seismically active and initially forming the western boundary of the No. 4 shaft pillar, was largely neutralised by first mining a wide strip between it and the rest of the shaft pillar. This procedure does not eliminate further stress induced seismic events along the structure, but spatially separates this particular hazard from active mine workings (Figure 10)

Conclusions are summarized as follows:

Time history analysis of åVa and moving median EI are useful to track the rockmass stress-strain behaviour during pillar mining.

Depending on the local geology and mining layouts, increased production rate can increase seismic risk by:

- causing a higher stress level in the immediate surrounds of the ore body and
- increase the frequency of larger events.

Statistical seismic hazard analysis (Gutenberg-Richter) at an early stage can indicate the probable nature of the rockmass response during pillar extraction.

ACKNOWLEDGEMENTS

The author wishes to thank the management of Western Holdings Mine for permission to publish this paper. Mr. J.C. Lategan, heading the Rock Engineering Department at the mine, provided essential information. The work was carried out as part of the GAP303 research project, sponsored by the Department of Minerals and Energy through the Safety in Mines Advisory Committee (SIMRAC). Clare Ilhan and Gerrit Kotze at ISS International helped with data preparation.

REFERENCES

1. LATEGAN, J.C. 1996. Final minutes of shaft pillar extraction review held at No. 1 Shaft canteen on 14 June 1996. Internal report, Western Holdings Mine, ref. WH226-96

2. MENDECKI, A.J. 1997. Seismic monitoring in mines. Chapman and Hall, London, 262 pp.

3. VAN ASWEGEN G, MENDECKI A J & FUNK C (1997). Application of quantitative seismology in mines in MENDECKI, A.J. (Ed) Seismic Monitoring in Mines. Chapman and Hall, London.

4. KJIKO, A, DRZEZLA, B & STANKIEWICZ, T. 1987. Bimodal character of the distribution of extreme seismic events in Polish mines. Acta Geophys. Pol. 35, 159-168.

5. SIMRAC, GAP 017 Final Report 1995.

APPENDIX 1: SEISMIC NOMENCLATURE

A brief summary of seismological terms used in this paper could be useful. A seismic event is a sudden, inelastic deformation episode of part of the rockmass. It radiates seismic (largely elastic) waves, which can be recorded by seismometers for the purpose of quantifying the seismic source. Four largely independent parameters describe a seismic event, namely time (T), location (X), seismic moment (M) and radiated seismic energy (E). Seismic moment relates to the physical size of the volume of rock, which underwent the deformation (mostly shear deformation). A local 'magnitude' is usually found by establishing an empirical relation between either E or M (or both) and the national magnitude, the latter being based on the Richter magnitude.

An increase in radiated seismic energy for constant seismic moment ('amount' of co-seismic strain), reflects an increase in the rate of co-seismic deformation, indicating that an increased driving force was required to cause the deformation. In terms of a simple shear mechanism (e.g. slip on a joint plane) this would happen if the rock strength or general level of stress increases. Thus a general increase in the E/M ratio of seismic events in a given rock volume is interpreted as reflecting an increase in the stress level. This is quantified by apparent stress:

Apparent stress [Pa]:. The ratio of radiated seismic energy to seismic moment multiplied by rigidity, μ, is called apparent stress, σ_A, and is recognised as a model independent measure of the stress change at the seismic source.

$$\sigma_A = \mu \frac{E}{M}$$

Energy Index: The notion of comparing the radiated energies of seismic events of similar moments can be translated into a practical tool called Energy Index (EI) - the ratio of the radiated energy of a given event (E) to the average energy released by events of the same seismic moment in the area of interest. A small or moderate

event with EI > 1 suggests a higher than average shear stress at its location. The opposite applies to the EI < 1 case.

$$EI = \frac{E}{\overline{E}(M)}$$

Apparent Stress Level [Pa]: To compare the general stress level between two areas, one could quote the coefficient b of the empirical line fit:

Log(E) = aLog (M) + b

This would, in general, be difficult to intuitively interpret. For this reason the concept of quoting the average σ_A for given seismic moment is suggested.

$\overline{\sigma_A} < M^{10} >$, or, "Apparent Stress Level" (ASL for brevity).

A convenient number for moment is chosen, e.g. 1E10 N.m - e.g. log(M) = 10 and the appropriate value of E is found, allowing the calculation of an apparent stress value, being the average apparent stress for the chosen value of moment. (See Fig. 7 in the text).

Apparent Volume [m^3]: Source volume V - the volume of co seismic inelastic deformation $\varepsilon = \Delta\sigma / \mu$ - can be estimated from $V = M / \Delta\sigma$. The apparent volume for a given seismic event scales the volume of rock with co seismic inelastic strain of an order of apparent stress over rigidity. The apparent volume V_A is less model dependant than the source volume V.

For more details, see Mendecki, 1997.